



ISSN: 2347-6567

## International Journal of Allied Medical Sciences and Clinical Research (IJAMSCR)

IJAMSCR | Vol.14 | Issue 1 | Jan - Mar -2026

www.ijamscr.com

DOI : <https://doi.org/10.61096/ijpar.v14.Iss1.2026.46-57>

### Research

## Applying deep learning techniques to identify tonsilloliths in panoramic radiography

**Dr. K. Dharani<sup>1\*</sup>, Dr. T. Madhavi Padhma<sup>2</sup>, Dr. KVNR Prathap<sup>3</sup>, Dr. Vengal Rao<sup>4</sup>,  
Dr. Srujan Kumar<sup>5</sup>, Dr. Darshika Chandini<sup>6</sup>**

*1-Student, 2-Professor and HOD, 3,4-Professor, 5,6-Senior Lecturer*

*1,2,3,4,5,6 Department of Public Health Dentistry, Mamata Dental College, Khammam, India*

\*Corresponding author: Dr. K. Dharani

Email: [karnavathdharani2002@gmail.com](mailto:karnavathdharani2002@gmail.com)

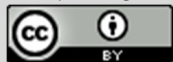


Published on: 30.01.2026

Published by:

Futuristic Publications

2026| All rights reserved.



[Creative Commons](#)

[Attribution 4.0 International](#)

[License.](#)

### Abstract

Tonsilloliths can be seen on panoramic radiographs (PRs) as deposits located on the middle portion of the ramus of the mandible. Although tonsilloliths are clinically harmless, the high risk of misdiagnosis leads to unnecessary advanced examinations and interventions, thus jeopardizing patient safety and increasing unnecessary resource use in the healthcare system. Therefore, this study aims to meet an important clinical need by providing accurate and rapid diagnostic support. The dataset consisted of a total of 275 PRs, with 125 PRs lacking tonsillolith and 150 PRs having tonsillolith. ResNet and EfficientNet CNN models were assessed during the model selection process. An evaluation was conducted to analyze the learning capacity, intricacy, and compatibility of each model with the problem at hand. The effectiveness of the models was evaluated using accuracy, recall, precision, and F1 score measures following the training phase. Both the ResNet18 and EfficientNetB0 models were able to differentiate between tonsillolith-present and tonsillolith-absent conditions with an average accuracy of 89%. Res Net 101 demonstrated underperformance when contrasted with other models. EfficientNetB1 exhibits satisfactory accuracy in both categories. The EfficientNetB0 model exhibits a 93% precision, 87% recall, 90% F1 score, and 89% accuracy. This study indicates that implementing AI-powered deep learning techniques would significantly improve the clinical diagnosis of tonsilloliths.

**Keywords:** Artificial intelligence; Deep learning; Dental digital radiography; Diagnostic imaging; Panoramic radiography.

### INTRODUCTION

Soft tissue calcifications (STCs) are radiopaque formations that occur as a result of the deposition of calcium salts.

They are typically asymptomatic and can be observed on panoramic radiographs (PRs) acquired during routine dental examinations<sup>1</sup>. Calcified lymph nodes,

tonsilloliths, cysticercosis, and vascular calcifications are examples of dystrophic calcifications that appear radiopaque in the head and neck region.

These calcifications are generally asymptomatic<sup>2</sup>. Tonsilloliths, often called tonsil stones, are calcified deposits that typically develop in the tonsil crypts of older persons, either on one side or both sides. In PRs, the presence of several radiopacities, resembling rice grains or irregular clusters, can be observed in the central sections of the ramus. It seldom attains significant dimensions, and its density is similar to that of compact bone. It is common for hard and soft tissue features to overlap on radiographic pictures in this anatomical location, which makes interpretation difficult. Dentists have the duty to identify tonsilloliths when they are overlapping with anatomical structures and to distinguish them from normal anatomical formations that appear radiopaque, dental abnormalities, bone abnormalities, foreign objects, artifacts, and other non-specific findings<sup>3,4</sup>.

PRs are utilized in dental practice due to their numerous benefits, including low radiation exposure, simple application, affordability, and convenient availability. They continue to hold their position as the predominant imaging technique utilized in the diagnosis and treatment planning of numerous oral and maxillofacial diseases<sup>5</sup>. Tonsilloliths should be identified during regular PRs and distinguished from clinical and anatomical abnormalities in order to establish the necessity for therapy.

Currently, artificial intelligence (AI) technologies are quickly gaining popularity in the field of dentistry. The efficient utilization of vast amounts of data is contingent upon the implementation of machine learning. As a

subfield of machine learning, deep learning employed artificial neural networks. The transmission of data representations layer by layer in these networks enables the development of greater abstraction and complexity<sup>6</sup>. Object detection, image classification, and segmentation are the most prevalent applications of Convolutional Neural Networks (CNNs) in this field. Convolutions are employed by these networks to derive features from images, such as colors, textures, edges, geometric shapes, and macroscopic structures. CNNs have been demonstrated to be extremely effective in both two-dimensional and three-dimensional radiographs in the field of dentistry, according to research<sup>7</sup>. This approach helps prevent inexperienced or careless physicians from overlooking asymptomatic lesions, leading to more accurate radiography interpretations. As a result, clinical diagnosis and treatment planning benefit from improved recall and reduced errors. Furthermore, its objective is to streamline the tasks of physicians, enhance patient care, and optimize treatment outcomes by actively supporting the education of physicians during their training<sup>8,9</sup>.

The objective of this study is to enhance clinical decision-making and optimize patient health management by utilizing AI-based deep learning techniques. This powered by AI approach will enhance the precision of tonsillolith diagnosis and reduce errors in clinical assessments.

**Aim:** To develop and evaluate a deep learning-based system for automatically detecting tonsilloliths on panoramic radiographs, with the goal of improving diagnostic accuracy and efficiency

**Objective:** The objective of this study is to enhance clinical decision-making and optimize patient health management by

utilizing AI-based deep learning techniques. This powered by AI approach will enhance the precision of tonsillolith diagnosis and reduce errors in clinical assessments.

## METHODOLOGY:

### Study Design:

This retrospective study analyzed digital panoramic radiographs to detect tonsilloliths using deep learning techniques.

### Objective:

The objective was to develop an AI-powered model for accurate and rapid diagnosis of tonsilloliths in panoramic radiographs.

### Data Collection Methods

- 275 panoramic radiographs (PRs) were collected, with 125 lacking tonsillolith and 150 having tonsillolith.
- Images were obtained from patients who underwent panoramic radiography at a dental hospital.
- Data was divided into training (80%) and testing (20%) sets.

### Data Analysis:

- ResNet and EfficientNet CNN models were evaluated for their learning capacity and compatibility.
- Performance metrics included accuracy, recall, precision, and F1 score.

- EfficientNetB0 model achieved 89% accuracy, 93% precision, 87% recall, and 90% F1 score <sup>1</sup>.

### Ethical Considerations:

- The study protocol was approved by the Ethics Committee of the Faculty of Dentistry.
- Informed consent was obtained from patients or their guardians.
- Patient data was anonymized to maintain confidentiality <sup>2</sup>.

### Limitations:

- Limited dataset size and quality may affect model generalizability.
- Deep learning models require extensive computational resources and expertise.
- Tonsillolith detection can be challenging due to overlapping anatomical structures <sup>3 1</sup>.

## RESULTS

A total of 200 students took part in this with with female (65%) and male of (34%) age of the participants ranging from 19 to 25 years in this study females were more likely to demonstrate perception in dissection room experience than male significantly interns and 3rd year showed greater familiarity with advanced applications than first 4th years and 2<sup>nd</sup> year.

| Age                |             |
|--------------------|-------------|
| minimum            | 19          |
| maximum            | 25          |
| mean               | 22.715      |
| standard deviation | 1.372294048 |

| Gender         |           |         |               |                    |
|----------------|-----------|---------|---------------|--------------------|
|                | frequency | percent | valid percent | cumulative percent |
| <b>male:</b>   | 69        | 34.5    | 34.5          | 34.5               |
| <b>female:</b> | 131       | 65.5    | 65.5          | 100                |
| <b>total:</b>  | 200       | 100     | 100           |                    |

| Year             |           |         |               |                    |
|------------------|-----------|---------|---------------|--------------------|
|                  | frequency | percent | valid percent | cumulative percent |
| <b>intern(5)</b> | 74        | 37      | 37            | 37                 |
| <b>BDS 1</b>     | 14        | 7       | 7             | 44                 |
| <b>BDS 2</b>     | 21        | 10.5    | 10.5          | 54.5               |
| <b>BDS 3</b>     | 59        | 29.5    | 29.5          | 84                 |
| <b>BDS 4</b>     | 32        | 16      | 16            | 100                |
| <b>total</b>     | 200       | 100     | 100           |                    |

| Distribution and comparison of responses based on gender |          |       |             |         |             |                  |             |
|--|----------|-------|-------------|---------|-------------|------------------|-------------|
| Item   | response | males |             | females |             | chi-square value | p-value     |
|  |          | n     | %           | n       | %           |                  |             |
| <b>Q1</b>  | 1        | 11    | 16.92307692 | 27      | 21.6        | 1.671584068      | 0.643269675 |
|  | 2        | 15    | 23.07692308 | 35      | 28          |                  |             |
|  | 3        | 27    | 41.53846154 | 42      | 33.6        |                  |             |
|  | 4        | 12    | 18.46153846 | 21      | 16.8        |                  |             |
| <b>Q2</b>  | 1        | 22    | 31.88405797 | 42      | 32.0610687  | 7.705163477      | 0.052514766 |
|  | 2        | 19    | 27.53623188 | 32      | 24.42748092 |                  |             |
|  | 3        | 15    | 21.73913043 | 44      | 33.58778626 |                  |             |
|  | 4        | 13    | 18.84057971 | 13      | 9.923664122 |                  |             |
| <b>Q3</b>  | 1        | 22    | 31.88405797 | 38      | 29.00763359 | 3.271130956      | 0.351680932 |
|  | 2        | 15    | 21.73913043 | 42      | 32.0610687  |                  |             |
|  | 3        | 26    | 37.68115942 | 37      | 28.24427481 |                  |             |
|  | 4        | 4     | 8.695652174 | 14      | 10.6870229  |                  |             |
| <b>Q4</b>  | 1        | 12    | 17.39130435 | 27      | 20.61068702 | 1.058468377      | 0.787108237 |
|  | 2        | 20    | 28.98550725 | 30      | 22.90076336 |                  |             |
|  | 3        | 26    | 37.68115942 | 50      | 38.16793893 |                  |             |
|  | 4        | 11    | 15.94202899 | 24      | 18.32061069 |                  |             |
| <b>Q5</b>  | 1        | 12    | 17.64705882 | 29      | 22.30769231 | 5.331853418      | 0.149048774 |
|  | 2        | 12    | 17.64705882 | 30      | 23.07692308 |                  |             |
|  | 3        | 19    | 27.94117647 | 43      | 33.07692308 |                  |             |
|  | 4        | 25    | 36.76470588 | 28      | 21.53846154 |                  |             |
| <b>Q6</b>  | 1        | 13    | 18.84057971 | 31      | 23.66412214 | 1.437254112      | 0.696825862 |
|  | 2        | 14    | 20.28985507 | 30      | 22.90076336 |                  |             |
|  | 3        | 29    | 42.02898551 | 52      | 39.69465649 |                  |             |
|  | 4        | 13    | 18.84057971 | 18      | 13.74045802 |                  |             |

|            |   |    |             |    |             |             |             |
|------------|---|----|-------------|----|-------------|-------------|-------------|
| <b>Q7</b>  | 1 | 11 | 15.94202899 | 27 | 20.76923077 | 1.099899786 | 0.777098276 |
|            | 2 | 20 | 28.98550725 | 34 | 26.15384615 |             |             |
|            | 3 | 27 | 39.13043478 | 45 | 34.61538462 |             |             |
|            | 4 | 11 | 15.94202899 | 24 | 18.46153846 |             |             |
| <b>Q8</b>  | 1 | 18 | 26.86567164 | 32 | 25.19685039 | 0.815597535 | 0.845732786 |
|            | 2 | 17 | 25.37313433 | 33 | 25.98425197 |             |             |
|            | 3 | 21 | 31.34328358 | 46 | 36.22047244 |             |             |
|            | 4 | 11 | 16.41791045 | 16 | 12.5984252  |             |             |
| <b>Q9</b>  | 1 | 17 | 24.63768116 | 21 | 16.8        | 4.212254756 | 0.239437812 |
|            | 2 | 20 | 28.98550725 | 47 | 37.6        |             |             |
|            | 3 | 28 | 40.57971014 | 43 | 34.4        |             |             |
|            | 4 | 4  | 5.797101449 | 14 | 11.2        |             |             |
| <b>Q10</b> | 1 | 14 | 21.21212121 | 26 | 20.15503876 | 2.178898438 | 0.536116671 |
|            | 2 | 20 | 30.3030303  | 30 | 23.25581395 |             |             |
|            | 3 | 19 | 28.78787879 | 50 | 38.75968992 |             |             |
|            | 4 | 13 | 19.6969697  | 23 | 17.82945736 |             |             |
| <b>Q11</b> | 1 | 15 | 22.72727273 | 28 | 22.04724409 | 0.718742284 | 0.86878697  |
|            | 2 | 20 | 30.3030303  | 32 | 25.19685039 |             |             |
|            | 3 | 21 | 31.81818182 | 45 | 35.43307087 |             |             |
|            | 4 | 10 | 15.15151515 | 22 | 17.32283465 |             |             |
| <b>Q12</b> | 1 | 19 | 27.94117647 | 18 | 13.74045802 | 11.07199083 | 0.011342896 |
|            | 2 | 9  | 13.23529412 | 41 | 31.29770992 |             |             |
|            | 3 | 27 | 39.70588235 | 45 | 34.35114504 |             |             |
|            | 4 | 13 | 19.11764706 | 27 | 20.61068702 |             |             |
| <b>Q13</b> | 1 | 7  | 10.44776119 | 15 | 11.71875    | 1.273107788 | 0.735528586 |
|            | 2 | 16 | 23.88059701 | 34 | 26.5625     |             |             |
|            | 3 | 28 | 41.79104478 | 57 | 44.53125    |             |             |
|            | 4 | 16 | 23.88059701 | 22 | 17.1875     |             |             |
| <b>Q14</b> | 1 | 9  | 13.23529412 | 21 | 16.27906977 | 0.591363455 | 0.898406636 |
|            | 2 | 22 | 32.35294118 | 38 | 29.45736434 |             |             |
|            | 3 | 26 | 38.23529412 | 52 | 40.31007752 |             |             |
|            | 4 | 11 | 16.17647059 | 18 | 13.95348837 |             |             |
| <b>Q15</b> | 1 | 13 | 20          | 18 | 14.63414634 | 2.853698551 | 0.414736295 |
|            | 2 | 14 | 21.53846154 | 37 | 30.08130081 |             |             |
|            | 3 | 30 | 46.15384615 | 48 | 39.02439024 |             |             |
|            | 4 | 8  | 12.30769231 | 20 | 16.2601626  |             |             |

$P \leq 0.05$  is statistically significant

| Distribution and comparison of responses based on year of study |          |              |             |               |             |                |             |               |        |            |             |                    |             |
|---|----------|--------------|-------------|---------------|-------------|----------------|-------------|---------------|--------|------------|-------------|--------------------|-------------|
| Item  | response | I<br>BD<br>S |             | II<br>BD<br>S |             | III<br>BD<br>S |             | IV<br>BD<br>S |        | INTE<br>RN |             | ChiSquare<br>Value | P-<br>Value |
|   |          | n            | %           | n             | %           | n              | %           | n             | %      | n          | %           |                    |             |
| <b>Q1</b>   | 1        | 2            | 14.28571429 | 1             | 5           | 7              | 13.7254902  | 5             | 15.625 | 23         | 31.08108108 | 18.31              | 0.106       |
|   | 2        | 4            | 28.57142857 | 8             | 40          | 17             | 33.33333333 | 11            | 34.375 | 11         | 14.86486486 |                    |             |
|   | 3        | 7            | 50          | 9             | 45          | 17             | 33.33333333 | 13            | 40.625 | 23         | 31.08108108 |                    |             |
|   | 4        | 1            | 7.142857143 | 2             | 10          | 10             | 19.60784314 | 3             | 9.375  | 17         | 22.97297297 |                    |             |
| <b>Q2</b>   | 1        | 5            | 35.71428571 | 6             | 28.57142857 | 22             | 37.28813559 | 8             | 25     | 23         | 32.85714286 | 9.77               | 0.637       |
|   | 2        | 3            | 21.42857143 | 9             | 42.85714286 | 12             | 57.14285714 | 8             | 25     | 19         | 27.14285714 |                    |             |
|   | 3        | 2            | 14.28571429 | 5             | 23.80952381 | 16             | 76.19047619 | 13            | 40.625 | 19         | 27.14285714 |                    |             |
|   | 4        | 4            | 28.57142857 | 1             | 4.761904762 | 9              | 42.85714286 | 3             | 9.375  | 9          | 12.85714286 |                    |             |
| <b>Q3</b>   | 1        | 3            | 21.42857143 | 6             | 28.57142857 | 18             | 30.50847458 | 10            | 31.25  | 23         | 31.08108108 | 9.22               | 0.684       |
|   | 2        | 6            | 42.85714286 | 9             | 42.85714286 | 18             | 30.50847458 | 6             | 18.75  | 18         | 24.32432432 |                    |             |
|   | 3        | 5            | 35.71428571 | 6             | 28.57142857 | 20             | 33.89830508 | 13            | 40.625 | 19         | 25.67567568 |                    |             |
|   | 4        | 0            | 0           | 0             | 0           | 3              | 5.084745763 | 3             | 9.375  | 14         | 18.91891892 |                    |             |
| <b>Q4</b>   | 1        | 1            | 7.14        | 2             | 9.52        | 16             | 27.12       | 5             | 15.63  | 15         | 20.27       | 15.44              | 0.218       |
|   | 2        | 3            | 21.43       | 6             | 28.57       | 16             | 27.12       | 10            | 31.25  | 15         | 20.27       |                    |             |
|   | 3        | 7            | 50          | 8             | 38.1        | 13             | 22.03       | 13            | 40.63  | 35         | 47.3        |                    |             |
|   | 4        | 3            | 21.43       | 5             | 23.81       | 14             | 23.73       | 4             | 12.5   | 9          | 12.16       |                    |             |
| <b>Q5</b>   | 1        | 8            | 57.14       | 5             | 23.81       | 10             | 16.95       | 9             | 28.13  | 9          | 12.16       | 10.82              | 0.5         |
|   | 2        | 2            | 14.29       | 4             | 19.05       | 11             | 18.64       | 6             | 18.75  | 19         | 25.68       |                    |             |

|            |   |   |       |   |       |    |       |    |           |    |       |       |       |
|------------|---|---|-------|---|-------|----|-------|----|-----------|----|-------|-------|-------|
|            | 3 | 1 | 7.14  | 5 | 23.81 | 21 | 35.59 | 7  | 21.8<br>8 | 28 | 37.84 |       |       |
|            | 4 | 3 | 21.43 | 7 | 33.33 | 17 | 28.81 | 9  | 31.2<br>5 | 18 | 24.32 |       |       |
| <b>Q6</b>  | 1 | 6 | 42.86 | 7 | 33.33 | 11 | 18.64 | 6  | 18.7<br>5 | 14 | 18.92 | 13.77 | 0.397 |
|            | 2 | 2 | 14.29 | 5 | 23.81 | 12 | 20.34 | 9  | 28.1<br>3 | 16 | 21.62 |       |       |
|            | 3 | 6 | 42.86 | 6 | 28.57 | 26 | 44.07 | 11 | 34.3<br>8 | 32 | 43.24 |       |       |
|            | 4 | 0 | 0     | 3 | 14.29 | 10 | 16.95 | 6  | 18.7<br>5 | 12 | 16.22 |       |       |
| <b>Q7</b>  | 1 | 1 | 7.14  | 3 | 14.29 | 10 | 16.95 | 8  | 25        | 16 | 21.62 | 8.96  | 0.709 |
|            | 2 | 3 | 21.43 | 6 | 28.57 | 14 | 23.73 | 10 | 31.2<br>5 | 21 | 28.38 |       |       |
|            | 3 | 5 | 35.71 | 7 | 33.33 | 27 | 45.76 | 9  | 28.1<br>3 | 24 | 32.43 |       |       |
|            | 4 | 5 | 35.71 | 4 | 19.05 | 8  | 13.56 | 5  | 15.6<br>3 | 13 | 17.57 |       |       |
| <b>Q8</b>  | 1 | 4 | 28.57 | 4 | 19.05 | 19 | 32.2  | 7  | 21.8<br>8 | 16 | 21.62 | 11.54 | 0.568 |
|            | 2 | 3 | 21.43 | 6 | 28.57 | 14 | 23.73 | 7  | 21.8<br>8 | 20 | 27.03 |       |       |
|            | 3 | 5 | 35.71 | 6 | 28.57 | 17 | 28.81 | 10 | 31.2<br>5 | 29 | 29.73 |       |       |
|            | 4 | 1 | 14.29 | 5 | 23.81 | 8  | 15.25 | 7  | 25        | 6  | 21.62 |       |       |
| <b>Q9</b>  | 1 | 3 | 21.43 | 2 | 9.52  | 10 | 16.95 | 8  | 25        | 15 | 20.27 | 14.64 | 0.612 |
|            | 2 | 3 | 21.43 | 6 | 28.57 | 18 | 30.51 | 10 | 31.2<br>5 | 30 | 40.54 |       |       |
|            | 3 | 7 | 50    | 6 | 28.57 | 20 | 33.9  | 13 | 40.6<br>3 | 25 | 33.78 |       |       |
|            | 4 | 1 | 7.14  | 5 | 33.33 | 10 | 18.64 | 1  | 3.13      | 1  | 5.41  |       |       |
| <b>Q10</b> | 1 | 1 | 7.14  | 5 | 23.81 | 11 | 18.64 | 9  | 28.1<br>3 | 14 | 18.92 | 10.03 | 0.612 |
|            | 2 | 4 | 28.57 | 6 | 28.57 | 13 | 22.03 | 8  | 25        | 19 | 25.68 |       |       |
|            | 3 | 6 | 42.86 | 7 | 33.33 | 25 | 42.37 | 8  | 25        | 23 | 31.08 |       |       |
|            | 4 | 3 | 21.43 | 3 | 14.29 | 8  | 16.95 | 7  | 21.8<br>8 | 15 | 24.32 |       |       |

|  |   |   |       |   |       |    |       |    |      |    |       |       |       |
|--|---|---|-------|---|-------|----|-------|----|------|----|-------|-------|-------|
| <b>Q1</b>                                  |   |   |       |   |       |    |       |    | 21.8 |    |       |       |       |
| <b>1</b>                                   | 1 | 3 | 21.43 | 4 | 19.05 | 11 | 18.64 | 7  | 8    | 18 | 24.32 | 7.92  | 0.843 |
|  | 2 | 3 | 21.43 | 6 | 28.57 | 20 | 33.9  | 7  | 8    | 16 | 21.62 |       |       |
|  | 3 | 5 | 35.71 | 8 | 38.1  | 20 | 33.9  | 10 | 31.2 | 5  | 23    | 31.08 |       |
|  | 4 | 3 | 21.43 | 3 | 14.29 | 4  | 13.56 | 7  | 25   | 15 | 23    |       |       |
| <b>Q1</b>                                  |   |   |       |   |       |    |       |    | 21.8 |    |       |       |       |
| <b>2</b>                                   | 1 | 2 | 21.43 | 3 | 14.29 | 12 | 21.88 | 7  | 8    | 13 | 17.57 | 7.09  | 0.843 |
|  | 2 | 4 | 21.43 | 7 | 33.33 | 13 | 21.88 | 7  | 8    | 19 | 25.68 |       |       |
|  | 3 | 6 | 35.71 | 8 | 38.1  | 22 | 37.5  | 12 | 37.5 | 24 | 32.43 |       |       |
|  | 4 | 2 | 21.43 | 3 | 14.29 | 11 | 18.75 | 6  | 18.7 | 5  | 18    | 24.32 |       |
| <b>Q1</b>                                  |   |   |       |   |       |    |       |    | 12.5 |    |       |       |       |
| <b>3</b>                                   | 1 | 1 | 14.29 | 2 | 9.52  | 5  | 12.5  | 4  | 12.5 | 10 | 13.51 | 7.09  | 0.871 |
|  | 2 | 6 | 28.57 | 5 | 23.81 | 13 | 28.13 | 9  | 28.1 | 3  | 17    | 22.97 |       |
|  | 3 | 5 | 42.86 | 8 | 38.1  | 24 | 40.63 | 13 | 40.6 | 3  | 35    | 45.95 |       |
|  | 4 | 2 | 14.29 | 5 | 28.57 | 15 | 18.75 | 6  | 18.7 | 5  | 10    | 18.92 |       |
| <b>Q1</b>                                  |   |   |       |   |       |    |       |    | 18.7 |    |       |       |       |
| <b>4</b>                                   | 1 | 3 | 21.43 | 2 | 9.52  | 7  | 18.75 | 6  | 5    | 12 | 16.22 | 11.21 | 0.593 |
|  | 2 | 4 | 28.57 | 7 | 33.33 | 20 | 31.25 | 10 | 31.2 | 5  | 19    | 25.68 |       |
|  | 3 | 6 | 42.86 | 9 | 42.86 | 23 | 25    | 8  | 25   | 32 | 43.24 |       |       |
|  | 4 | 1 | 7.14  | 3 | 14.29 | 8  | 25    | 7  | 25   | 10 | 14.86 |       |       |
| <b>Q1</b>                                  |   |   |       |   |       |    |       |    | 15.6 |    |       |       |       |
| <b>5</b>                                   | 1 | 2 | 14.29 | 3 | 14.29 | 7  | 15.63 | 5  | 3    | 14 | 18.92 | 13.58 | 0.559 |
|  | 2 | 5 | 35.71 | 6 | 28.57 | 12 | 28.13 | 9  | 28.1 | 3  | 19    | 25.68 |       |
|  | 3 | 5 | 35.71 | 9 | 42.86 | 23 | 43.75 | 14 | 43.7 | 5  | 27    | 36.49 |       |
| <i>P≤0.05 is statistically significant</i> |   |   |       |   |       |    |       |    |      |    |       |       |       |

## Discussion

The current study examined a variety of CNN models to evaluate their efficacy,

learning capacity, and complexity in the context of tonsillolith identification. To the best of our knowledge, there is no research on the identification of tonsilloliths in the



literature. We are of the opinion that this investigation will be the first to address this subject.

Deep learning models have been employed in numerous published research projects to explore different aspects of dentistry practice. AI systems are being utilized to research the identification of dental anomalies, such as taurodontism<sup>13</sup>. Jae-Hong<sup>14</sup> showed that CNN architectures may be utilized for identifying and categorizing dental implant systems. However, the number of studies that have employed deep learning techniques to identify calcifications in soft tissues of the head and neck is relatively small<sup>15:16:17:18</sup>. Ishibashi et al.<sup>19</sup> employed deep learning techniques to identify sialoliths in panoramic radiography. They developed three distinct models and assessed the accuracy of these models in detecting sialoliths by organizing the datasets in a differing manner. They attained the highest detection rates (recall: 85%, precision: 100%, and F score of 91.9%) for sialoliths in panoramic radiographs with two models. Tonsilloliths were identified by EfficientNetB0 in our investigation with a recall rate of 87%, precision of 93%, and F score of

90%. Despite the fact that our dataset was smaller, the recall values for ResNet18 and EfficientNetB0 in our study were 87%, which was slightly higher than those in the study conducted by Ishibashi et al.<sup>19</sup>. In contrast, the highest precision value achieved in our analysis was 90% (ResNet18 and EfficientNetB0), which was lower than that of the previous study. The different number of epochs employed in the investigations may be the cause of this situation. Vinayahalingam et al.<sup>20</sup> investigated the detection of carotid artery calcifications on panoramic radiographs through the application of deep learning

techniques. The results indicate that the proposed method, which was designed using Faster R-CNN and Swin Transformer, achieved an F1 score of 89%, a recall of 88%, and a rate of precision of 89%. It is possible to conclude that the study results are consistent when observed in comparison to the results of our study, as similar values were obtained.

By enabling visualization of the maxillary and mandibular arches and their adjacent structures on a single film, panoramic radiography is an extensively utilized technique across all domains of dentistry<sup>10:21</sup>. Soft tissue calcifications, including tonsilloliths, sialoliths, lymph node calcifications, and calcified atheroma plaque, may also be detected via panoramic imaging. However, it is probable that inexperienced physicians will fail to notice it<sup>15</sup>. According to studies utilizing panoramic imaging, tonsillitis prevalence ranged from 7.3 to 13.4%<sup>22:23:24:25</sup>. Studies using computed tomography have shown a higher occurrence rate. Fauroux et al.<sup>26</sup> reported a prevalence rate of 24.6%, whereas Oda et al.<sup>22</sup> reported a higher prevalence rate of 46.1%. The identification of this relatively common soft tissue calcification is accomplished through the examination of its spatial distribution on the panoramic film. They are capable of being superimposed on the mandible as well as the adjacent soft tissue. Distinguishing palatine tonsilloliths from parotid sialoliths, submandibular salivary ducts, and phleboliths, which are calcified structures that should not be present, is a critical medical judgment for physicians<sup>24</sup>.

The application of AI techniques can provide physicians with support in making decisions pertaining to patient care<sup>27</sup>. Song et al.<sup>15</sup> conducted a study comparing the reading speed and detection success of

two oral and maxillofacial radiologists and two general dentists when analyzing panoramic films with soft tissue calcification (sialolith, lymph node calcification and carotid artery calcification) using Fast R-CNN. They reported a recall of 77.4%, and a specificity of 71.4% for carotid artery calcification (CAC). The study also showed that expert radiologists took less time to analyze films during the second reading, as compared to the first reading conducted without the use of AI. Additionally, general dentists exhibited improved ability to detect STCs. Kats et al.[16](#) employed the Fast R-CNN technique on a limited dataset to ascertain the presence of CAC on PRs. Using a limited set of 65 panoramic photos, they were able to identify CACs with a recall of 75%, a specificity of 80%, and an accuracy of 83%. Amitay et al.[17](#) used 500 PRs in their study to automatically identify CACs using a CNN method implemented using a transfer learning technique. The algorithm employs deep learning CNN with a transfer learning approach. It successfully obtained accurate labels for each corner and achieved a recall of 82% and a specificity of 97% for individual arteries. Additionally, it achieved a recall of 87% and a specificity of 97% for individual patients. Ajami et al.[18](#) favored the use of CBCT images for the automated identification and localization of CACs. Their analysis yielded a recall of 94.2% and a specificity of 96.5%. The ResNet18 model exhibited outstanding classification accuracy for both the tonsillolith-absent and tonsillolith-present classes in our investigation. The precision for both tonsillolith-absent and tonsillolith-present classes ranged from 85 to 93%. The recall ranged from 92 to 87%. The F1 score ranged from 88 to 90%. The accuracy for both classes was 89%. Furthermore, it has a lower FN ratio when compared to other

models. Although the ResNet101 model shows impressive accuracy in identifying tonsillolith, it also has a notable FP rate. The EfficientNetB1 model has a notable level of precision in both the tonsillolith-absent and tonsillolith-present groups, achieving an accuracy of 84%. Conversely, the EfficientNetB0 model has demonstrated exceptional accuracy, particularly in detecting tonsillolith instances. When evaluating the overall performance, the EfficientNetB0 model exhibits a comprehensive and strong performance with a precision of 93%, a recall of 87%, a F1 score of 90%, and an accuracy of 89%. However, the ResNet and EfficientNetB1 models exhibit distinct strengths and weaknesses. The high performance of the EfficientNetB0 model in the limited size and unbalanced class distribution dataset used in the study can be related to some of the technical features of its architectural structure. The EfficientNet architecture uses a compound scaling approach in which network dimensions such as depth, width, and resolution are scaled together and evenly. In this way, the model can maintain high accuracy with less computational cost while maintaining parameter efficiency. In addition, due to its smaller and optimized architecture, EfficientNetB0 can be more resistant to overfitting and show a more stable generalization performance on small-to-medium-sized data sets. The relatively small number of parameters makes it easier for the model to learn more robustly, especially in health data sets with a limited number of samples. EfficientNetB0 has been able to achieve high F1 scores and accuracy values in both tonsillolith-present and -absent cases as a result of these technical advantages.

The implementation of our proposed model in the dental clinic will assist inexperienced dentists in the identification

of tonsilloliths during radiological examinations, thereby preventing the need for unnecessary radiological investigations. In the literature, accuracy rates of 85% and higher in assistive decision support systems are seen as encouraging<sup>28,29</sup>. Since our study has an average accuracy of 89%, it serves as a significant and useful starting point for situations like diagnosing tonsilloliths. However, we would like to emphasize that this performance should be positioned as a supportive tool rather than completely taking over the physician's decision-making processes. In this direction, it is aimed to test the model in larger and multi-center data sets and to increase its clinical validity by using it together with expert evaluations in future studies.

Our study has some limitations. We utilized panoramic imaging to identify tonsilloliths. Panoramic radiography is a frequently utilized technology in dentistry that enables the visualization of both the upper and lower dental arches, as well as the surrounding structures, on a single image. Nevertheless, it is imperative that we should not disregard any alterations that may arise as a result of the patient's location<sup>30</sup>. The PRs utilized in our investigation were exclusively obtained from a single center. We included cases in which the presence of tonsilloliths was accepted by two oral and maxillofacial radiologists, as we did not re-evaluate the cases with three-dimensional imaging. Consequently, our dataset was restricted. Additionally, inter-observer variability analysis was not conducted due to the concurrent nature of the evaluation. The probability of obtaining successful results will be increased by incorporating multicenter studies into the dataset. Additionally, all PRs were acquired using the same device. It is uncertain how the model's performance would be impacted,

as images obtained from various devices were not utilized. The diagnosis of tonsilloliths was limited to cases in which two dentomaxillofacial radiologists reached a consensus on panoramic images in this study. There is a possibility that certain cases were misidentified, as verification was not conducted using three-dimensional imaging. Multidetector computed tomography or cone-beam computed tomography imaging may be required to ascertain the location of a suspected tonsillolith<sup>10</sup>. Nevertheless, this may lead to an elevated level of radiation exposure for the patient. We incorporated tonsillolith cases that were inadvertently identified on panoramic films that were obtained from patients for the purpose of investigation in our study. We claim that three-dimensional imaging has the capability to retrieve a more extensive collection of data as a result of its greater prevalence in computed tomography scans. Therefore, it is intended to conduct future research on CBCT images that utilize a more extensive dataset. Furthermore, it is intended to improve the interpretability of deep learning models by employing explanatory visualization techniques, including Grad-CAM++ and comparable methodologies. It is anticipated that these methods will significantly enhance the assessment of the reliability of model decisions, particularly in the field of medical imaging. In the same vein, semi-supervised learning approaches are also being investigated for future research, as the labeling process necessitates both time and expertise. It is anticipated that these methods will enhance the efficacy of systems that operate with restricted data and lower the annotation burden by enabling the more efficient utilization of unlabeled data.

## Conclusion

It is possible to train a dependable deep learning model to identify tonsilloliths on PRs, which would be a beneficial resource for oral healthcare professionals who are not familiar with STCs in the head and neck region. Our study has limitations such as being conducted with a limited dataset and only twodimensional imaging. Additional research is required to verify the clinical applicability and efficacy of this model. Future studies using data from multiple centers and a larger dataset size are important for making the model more reliable and applicable, especially when using threedimensional imaging for testing.

Nevertheless, the results indicate that deep learning methods supported by AI have significant potential to enhance the precision of clinical diagnosis of tonsilloliths and minimize errors.

**Data availability :** The data that support the findings of this study are available from Dicle University Faculty of Dentistry, but restrictions apply to the availability of these data, which were used under license for the current study and so are not publicly available. Data are, however, available from the corresponding author upon reasonable request and with permission from the Dicle University Faculty of Dentistry.

neck region. It is crucial to radiologically identify tonsilloliths in order to differentiate them from other abnormalities that necessitate treatment and to prevent the need for superfluous radiological evaluations.

## References

1. Avsever, H. & Orhan, K. Calcifications affecting the jawbone and surrounding tissues. *Turk. Clin. J. Oral Maxillofac. Radiol-Special Top.* 4, 43–52 (2018).
2. Parihar, A. et al. Calcific islands: A cone-beam computed tomography review of soft-tissue calcifications in head-and-neck region. *J. Oral Maxillofacial Radiol.* 8, 30–35 (2020).
3. Aghdasi, M. M., Valizadeh, S., Amin-Tavakoli, N. & Bakhshandeh, H. Tonsilolith in routine panoramic radiographies; is it a common incidental finding? *Iran. J. Radiol.* 9, 109–110 (2012).
4. Annapoorani, S., Thamby, J. R. & Christy, W. A retrospective diagnostic study of prevalence of orofacial calcifications using panoramic radiograph: to insinuate the unseen. *J. Clin. Experimental Dentistry.* 15, e289 (2023)
5. Privato, M. et al. Are panoramic images a good tool to detect calcified carotid atheroma?? A systematic review. *Biology* 11, 1684 (2022).